Version of Record: https://www.sciencedirect.com/science/article/pii/S0924424721006166
Manuscript_5f700beb31d2b120911fd7496936883b

# Analysis and comparison of the Core-to-Valence Luminescence mechanism in a large CLYC crystal under neutron and γ-ray irradiation through optical filtering selection of the scintillation light

F. Ferrulli[1,2,*], M. Caresana[3], F. Cova[4], S. Gundacker[2,^], N. Kratochwil[2,5], R. Pots[2], M. Silari[2], A. Vedda[4], I. Veronese[6], G. Zorloni[2,3]

[1] *Université de Caen Normandie, 14032 CAEN 5, France*

[2] *CERN, 1211 Geneva 23, Switzerland*

[3] *Department of Energy, Polytechnic of Milan, via Lambruschini 4, 20156, Milan, Italy*

[4] *Department of Materials Science, University of Milano – Bicocca, via Cozzi 55, 20125, Milan, Italy*

[5] *University of Vienna, Universitaetsring 1, 1010 Vienna, Austria*

[6] *Department of Physics, University of Milan and INFN, via Celoria 16, 20133, Milan, Italy*

[*] *Corresponding author*

*^ Present address: Department of Physics of Molecular Imaging Systems, Institute for Experimental Molecular Imaging, RWTH Aachen University, Forckenbeckstrasse 55, 52074 Aachen, Germany.*

## Abstract

$^{7}$Li enriched $Cs_2LiYCl_6:Ce^{3+}$ (CLYC) is a promising inorganic scintillator for real-time γ-ray and fast neutron spectrometry. The neutron/γ-ray discrimination is usually accomplished exploiting the different quenching effects of high Linear Energy Transfer (LET) particles on different scintillation mechanisms, usually by means of the time analysis of the pulse shape. In principle, the emission wavelength information could be used to address the same task. However, a systematic study of the correlations between the CLYC decay time, its radio-luminescence spectrum and the LET of the impinging particle has not yet been performed. We therefore investigated the CLYC scintillation process under neutron and γ-ray irradiation, correlating the time response to the scintillation wavelength spectrum using a 1–inch right cylinder > 99% $^{7}$Li enriched CLYC. We found that the relative intensity of the Core to Valence Luminescence (CVL) is almost constant with photons in the energy range 20–660 keV, *i.e.* 0.5–5 keV/µm LET, and is only partially quenched by neutrons. Instead, the direct electron-hole capture scintillation mechanism is completely cut under neutron irradiation. The luminescence in between the deep-Ultraviolet and the Near Ultraviolet region (250-350 nm) might be attributed to both the CVL and the host luminescence, also in thick highly $Ce^{3+}$-doped crystals.

**Keywords –** CLYC, Core to Valence Luminescence, wavelength-based discrimination, pulse shape analysis, radioluminescence, Time Correlated Single Photo Counting

## 1. Introduction

The $Cs_2LiYCl_6:Ce^{3+}$ (CLYC) is a promising inorganic scintillator for γ-ray spectrometry and neutron detection, with good neutron/γ-ray (n/γ) discrimination capability. CLYC rather good γ-ray spectrometry capabilities are due to its density (3.3 g/cm$^3$), $Z_{eff}$ (54) and energy resolution, about 5% at 662 keV [1,2]. Its fast neutron spectrometry properties were recently demonstrated for $^{7}$Li enriched crystals [3,4]. The reactions involved are $^{35}Cl(n,p)^{35}S$ and $^{35}Cl(n,\alpha)^{32}P$ below 15 MeV. The n/γ

discrimination can be performed through Pulse Shape Discrimination (PSD) by exploiting the different decay times of the scintillator when irradiated with neutrons and photons.

The good PSD capability of CLYC is mainly ascribed to the presence of the Core-To-Valence Luminescence (CVL) [5], a scintillation mechanism that, according to the literature, is selectively quenched by high Linear Energy Transfer (LET) particles, such as the reaction products emitted after neutron capture on $^{35}Cl$ [4,6]. These reaction products completely quench the CVL mechanism, causing a different time profile of the de-excitation process (and consequently of the detected signal) when the crystal is excited by neutrons rather than by γ-rays.

The CVL (also called cross-luminescence or Auger free luminescence) is an ultra-fast mechanism where an electron from the core band is excited into the conduction band. The consequent hole produced in the core band recombines with an electron of the valence band. Since the valence band is filled with electrons, the recombination probability is large resulting in a fast process [7]. The CVL is a competitive radiative de-excitation process with a decay time faster than that of the other three scintillation mechanisms present in CLYC, described below [8,9]. In CLYC, the CVL has a decay time of the order of 1-5 ns and is characterized by the emission of photons in between the deep-Ultraviolet (UV) and Near Ultraviolet (NUV) region (225-330 nm) [10,11]. The fast (direct electron-hole capture) and intermediate (binary electron-hole recombination mediated by the formation of a trapped hole centre, usually called $V_k$ complex [12]) mechanisms are related to the $Ce^{3+}$ de-excitation, and are characterized by a decay time of the order of 50 ns and 500 ns respectively. Both the fast and intermediate mechanism emit in the $Ce^{3+}$-related spectral range, *i.e.* between 350 nm and 450 nm [9]. The slowest mechanism is related to the host luminescence, with the formation of the so called self trapped excitons (STEs), and is characterized by a decay time of several μs [11,12]. In doped thick crystals, the STEs preferentially de-excite on $Ce^{3+}$, hence in the range 350-450 nm, but the decay constant is still governed by the STE migration dynamics, with a half life of a few microseconds [12]. Figure 1 shows a schematic of the energy levels of each scintillation mechanism (plots (c), (d) and (e) were taken from [12]). Plot (a) shows the CVL, plot (b) the fast $Ce^{3+}$ emission, usually ascribed to γ-ray irradiation only. Plot (c) shows the intermediate mechanism, *i.e.* the $V_k$ centre transferring its energy to the $Ce^{3+}$. The STE is represented both as a luminescence centre itself (plot (d)) and when it transfers its energy to the $Ce^{3+}$ (plot (e)).

Since the CVL emission occurs in a different spectral region than the $Ce^{3+}$ de-excitation, in principle the spectral information can be used to perform particle discrimination [13–15]. Considering that the CVL is observed only under photon irradiation, a CVL-selective optical filter should allow distinguishing a photon-induced signal from a neutron-induced one. However, a systematic study of the correlations between the CLYC decay time, its spectral information and the LET of the impinging particle has not yet been performed.

We therefore investigated the CVL behavior when the crystal is excited by neutrons and photons, correlating the time response to the scintillation wavelength spectrum. The analysis was carried out following two different methods: 1) by measuring the X-ray and γ-ray excited radio-luminescence (RL) spectra at different photon energies, and 2) by performing a pulse shape analysis of the signal produced by the interaction of γ-rays and neutrons, using both a photomultiplier tube (PMT) and a Time Correlated Single Photon Counting (TCSPC) technique [16,17]. All measurements were repeated with and without an optical filter in between the crystal and the sensor. The filter was chosen to select only the CVL-related spectral region. This allowed investigating the effects of the LET of the impinging particles on the specific scintillation mechanisms.

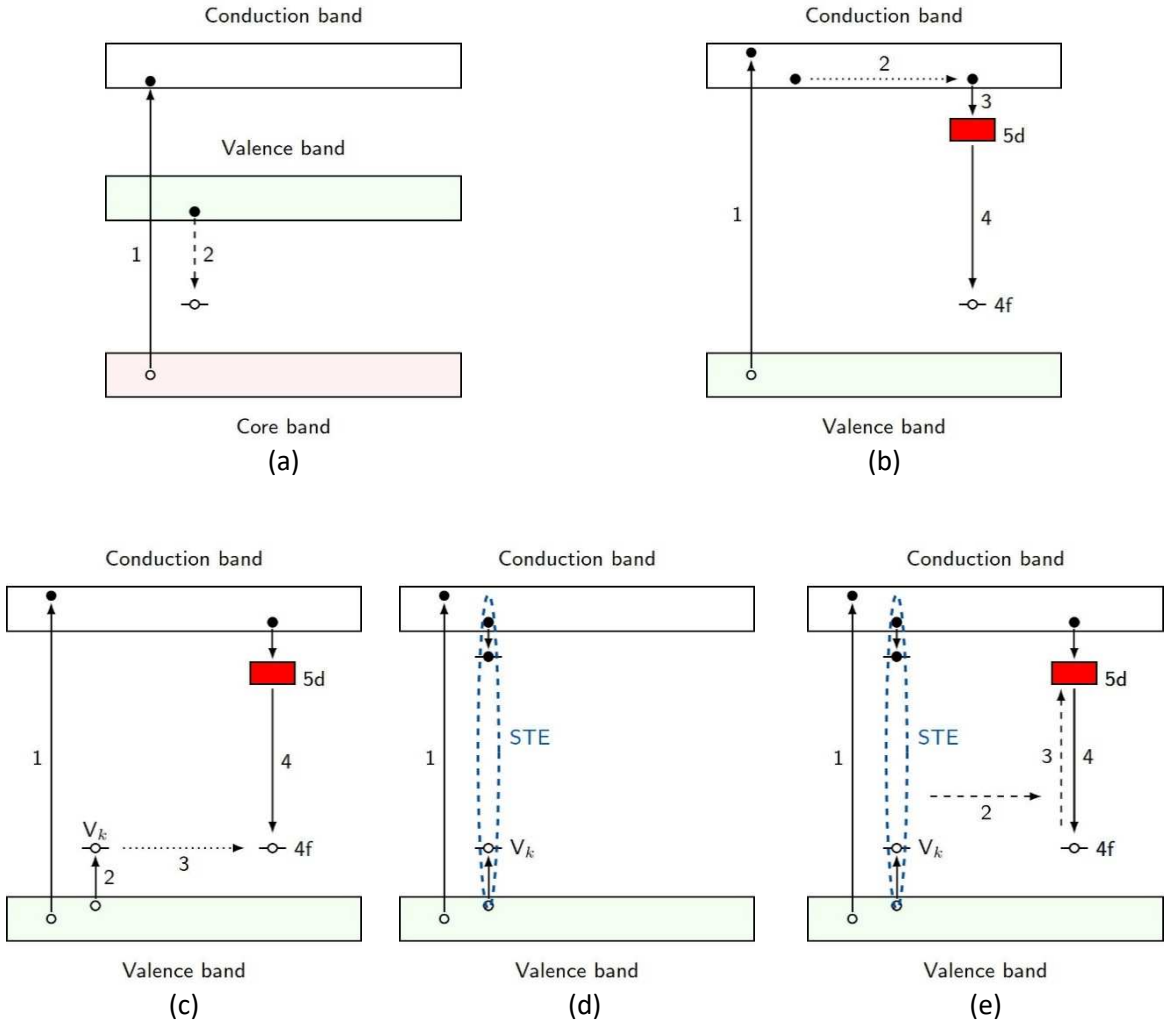


*Figure 1. Scintillation mechanisms in CLYC [12]. (a) Excitation of an electron from the core band to the conduction band and subsequent formation of a hole (1); the hole in the core band then recombines with a valence electron (2) causing the emission of the CVL light. (b) Excitation of an electron from the valence to the conduction band (1); the electron then migrates (2), reaching a $Ce^{3+}$ recombination site (3), with the subsequent radiative de-excitation (4). (c) Excitation of an electron from the valence to the conduction band (1) leaving a hole in the valence band; the hole is then trapped in a positive $V_k$ centre, forming a $Cl_2^-$ molecular complex (2). This defect thermally migrates (3) to a $Ce^{3+}$ centre forming a $Ce^{4+}$ or a $Ce^{3+}$ + $V_k$ complex. Eventually, the new centre recombines with an electron from the conduction band (4). (d*) Excitation of an electron from the valence to the conduction band and formation of a $V_k$ complex (1); a free electron is then trapped forming a STE complex, which can recombine radiatively. *(e) After the formation of the STE (1), this complex thermally migrates to a $Ce^{3+}$ centre (2). The STE can de-excites transferring its energy to a $Ce^{3+}$ centre (3), which subsequently recombines (4).*

## 2. Materials and methods

The measurements were performed with a 1–inch right cylinder CLYC scintillator enriched in $^7$Li to > 99%, purchased from Radiation Monitoring Devices [18]. The crystal is hygroscopic and therefore encapsulated in an aluminum housing provided with a single quartz window. The filter employed is an Asahi Spectra XUV0325 Shortpass Optical filter (Ø 25 mm, wavelength cut-off 325 nm) [19]. Its

transmittance was measured with an Agilent Varian Cary 50 spectrophotometer ranging from 190 nm to 1100 nm.

### 2.1 Radio-luminescence measurement setup

The first RL measurements were performed at the University of Milano – Bicocca. The measurement system is made of a liquid nitrogen-cooled, back-illuminated and UV-enhanced charge-coupled device (CCD) (Jobin-Yvon Spectrum One 3000). The CCD is coupled with a monochromator (Jobin-Yvon Triax 180) with a 100 grooves/mm grating. The RL excitation was obtained by X-ray irradiation using a Philips PW2274 X-ray tube with a tungsten anode and a Be-window, operated at 20 kV.

The second set of measurements employed a portable Back-thinned CCD Array Spectrometer Prime X (B&W TEK) [20]. A portable device was used for the irradiations performed at the calibration laboratory of the Polytechnic of Milan. X-ray fields were produced via a high-stability Seifert ISOVOLT 320/10 X-ray generator (maximum voltage 300 kV). The tube provides the complete ISO 4037 standard X-ray series radiation qualities [21]. In particular, the quasi-monoenergetic Narrow series (N-series) were employed. The N-series radiation qualities are recommended for the study of the energy dependence of the response of dosimeters [21]. $\gamma$-ray fields were produced by a certified 370 GBq $^{137}$Cs isotopic source. The scintillation light emitted by the crystal was sent to the spectrometer through an optical fiber cable. The fiber and the crystal were coupled using a black cone and a tailored 3D printed assembly to optimize the light collection and reduce the light losses. The spectrometer was controlled via a laptop.

### 2.2 Setup with the ultra-fast H6610 Hamamatsu PMT

For the analysis of the CVL time behavior, the Hamamatsu H6610 Bialkali PMT was selected for both its time response and its spectral response [22]. According to its datasheet, at 25 °C the PMT is characterized by a rise time of 0.7 ns and by a transit time spread of 0.16 ns. These values must be compared to the characteristic decay constants of the CLYC scintillation process. The observed shape of the electric signal on an oscilloscope coupled to the PMT is indeed given by the convolution of the time response of the PMT itself and the decay time of the scintillator. In this case, the contribution of the PMT can partially influence the precise determination of the CVL decay time (0.7 ns *versus* 1–5 ns) but for the other scintillation mechanisms its influence is completely negligible, as they all decay with half life > 50 ns.

Besides being characterized by a very short decay time, the CVL mechanism is observed in between the deep-UV and NUV wavelength range (250-350 nm). The quantum efficiency of the H6610 PMT varies from about 10% to 20% from roughly 200 nm up to 430 nm [22]. The window material of the H6610 PMT is made of silica glass, which transmits ultraviolet light down to 160 nm. On the contrary, the window material of commonly used PMTs consists of borosilicate glass, which transmits light only down to 300 nm [23]. The CLYC was coupled to the H6610 PMT through an optical grease (Rhodorsil Pate 7). The effective area of the PMT photocathode (20 mm diameter) was completely covered by the crystal surface whose diameter is 25.4 mm. The PMT was supplied with -2500 V, and the output connected to a Teledyne LeCroy Waverunner 8104 Oscilloscope (1 GHz, 20 GSamples/s) with a 50 Ω termination. The PMT and the crystal were placed inside a light-tight and thermally regulated chamber kept at 18 °C. When the optical filter was interposed between the PMT photocathode and the CLYC, a thin layer of the optical grease was applied on both surfaces of the filter for optical coupling.

The irradiations were performed employing a $^{137}$Cs source (3.31 MBq) and an unshielded Am-Be neutron source (359.03 MBq).

### 2.3 Time Correlated Single Photo Counting (TCSPC) setup

The TCSPC technique is specifically aimed for precise rise and decay time measurements of inorganic scintillators [16,17]. A $^{22}Na$ $\beta^+$ source was interposed between the CLYC and a fast detection system called start detector. The start detector is composed of a 2 mm × 2 mm × 5 mm LSO:Ce crystal coupled to an Hamamatsu Photonics K.K. (HPK) S13360-3050 Silicon Photomultiplier (SiPM) with a Meltmount thermoplastic, connected to a NINO readout board [24]. On the other side, the CLYC faced a Vacuum Ultraviolet single–photon avalanche diode (VUV–SPAD) from Fondazione Bruno Kessler, called stop detector ([25]). A SPAD is a photodiode operating in Geiger mode as an on-off switch triggered by a photon arriving on its surface. A SiPM is actually a dense array of independent SPADs, whose function is to count the number of photons reaching the SiPM surface [26]. In the hereby described setup, the CLYC and the stop detector (the VUV–SPAD) were not optically coupled [27].

The TCSPC technique works as follows (Figure 2). When one of the two annihilation γ-rays emitted in coincidence by the source is detected in the start detector, the time measurement starts. If the second γ-ray interacts with the crystal facing the stop detector, the scintillation produces several visible photons following its characteristic decay time statistics. The time measurement stops when the first scintillation photon reaches the stop detector. Saving a large number of events and plotting them on a histogram, the decay time of the scintillator is reconstructed in terms of number of counts *versus* emission time [16,17].

The measurement was performed with and without the filter. In the former case, the filter was interposed between the CLYC and the stop detector, at a distance of a few centimeters from both. Because of the smaller dimensions of the stop detector (a few tens of $\mu m^2$) compared to the surface of the filter (Ø 25 mm), it is reasonable to assume that the light reaching the photodetector was correctly filtered.

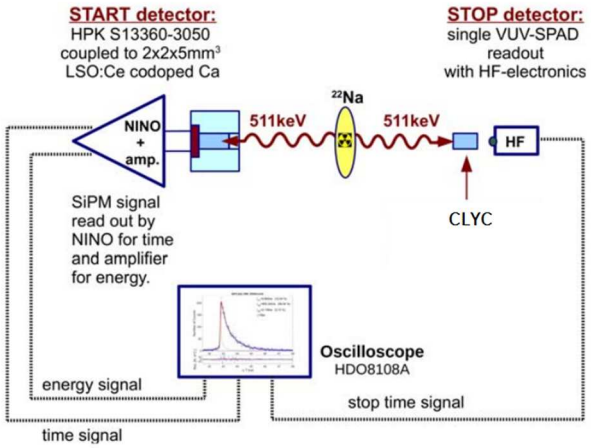


*Figure 2. The TCSPC setup with the CLYC crystal* [27].

## 3. Results and discussion

### 3.1 Radioluminescence spectra

Figure 3 shows the results of the RL characterization of the crystal performed at the University of Milano - Bicocca. The X-ray tube was operated at 20 kV. The RL emission spectrum was corrected for the background and for the spectral response of the detection system. The resulting spectrum shows

the characteristic doublet peak due to the $Ce^{3+}$ emission in the 340-500 nm range, peaked at 375 nm and 395 nm. A band is also revealed at around 300 nm, which is usually attributed to the CVL scintillation mechanism [8,28]. The relative intensity of the CVL mechanism with respect to the total scintillation light was quantified as the ratio of the area under the CVL portion of the spectrum (between 260 nm and 330 nm) over the area under the entire emission spectrum (between 260 nm and 500 nm). The CVL contribution is about 5% of the total signal. Figure 3 also shows the filter transmittance. It can be observed that the filter is selective to the CVL emission and completely cuts the $Ce^{3+}$ emission region.

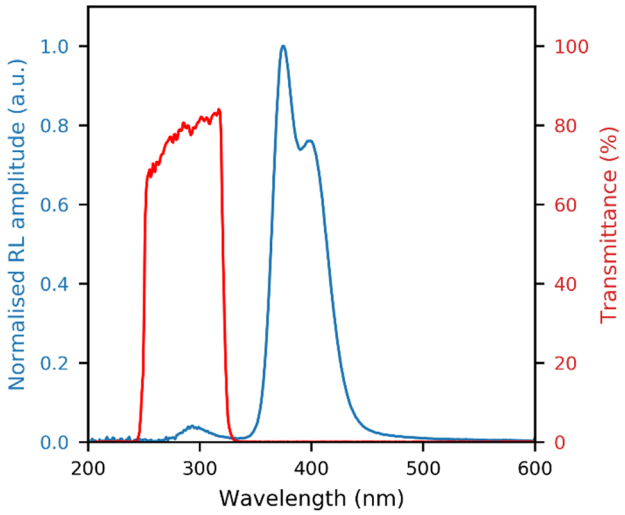


*Figure 3. Left y-axis: RL emission spectrum in CLYC irradiated with the X-ray tube operated at 20 kV. Right y-axis: measured transmittance of the Asahi Shortpass filter.*

Figures 4 and 5 show the results obtained at the Polytechnic of Milan. The spectra are background corrected and normalized to their maximum. The background was calculated as the average value of counts in the 800-900 nm region. The spectra are not corrected for the spectral response of the detector, because the response of the CCD was not characterized below 350 nm. However, a comparison in relative terms is still valid since the experimental setup was the same for all irradiations performed at the Polytechnic.

Figure 4 shows the RL spectra measured irradiating the CLYC with the $^{137}Cs$ source with and without the optical filter. The measurement demonstrates the proper selectivity of the filter in cutting the $Ce^{3+}$-related emission. Figure 5 shows the RL spectra obtained irradiating the crystal at different X-ray energies and with $^{137}Cs$ photons. Most authors working on the CLYC characterization generally agree that the CVL mechanism is selectively quenched only by high-LET particles such as neutron capture products. However, to the best of our knowledge the LET dependence of the RL spectral emission under γ-ray irradiation has never been studied. If a dependence of the CVL on LET in the tested 0.5–5 keV/µm range exists, the shape of the scintillation spectrum must vary as a function of the photon energy. Figure 6 shows the LET versus photon energy in the selected energy range.

If a dependence exists, methods based on the CVL suppression for neutron identification might return wrong results, *i.e.* low-energy photon-induced events could be misinterpreted as neutron-induced ones. This should be particularly critical in the case of a system using an optical-based discrimination readout. The curves shown in figure 5 do not reveal any dependence of the CVL mechanism on the energy of the incident photons.

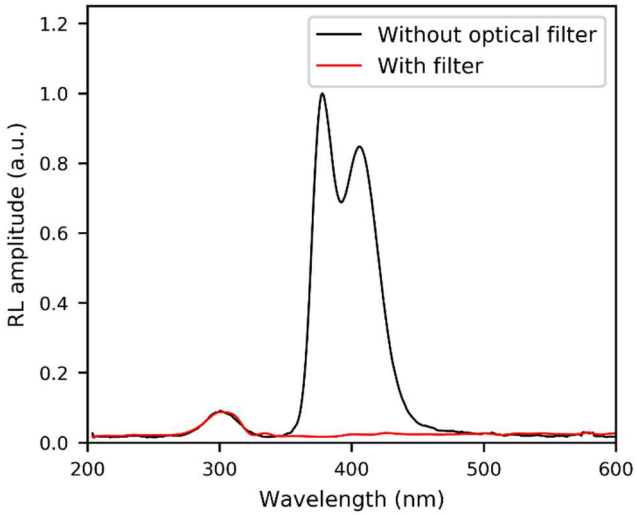


211

212 *Figure 4. RL emission spectrum in CLYC irradiated with the $^{137}$Cs source, measured with and without*
213 *the Asahi Shortpass filter between the crystal and the optical fiber.*

214

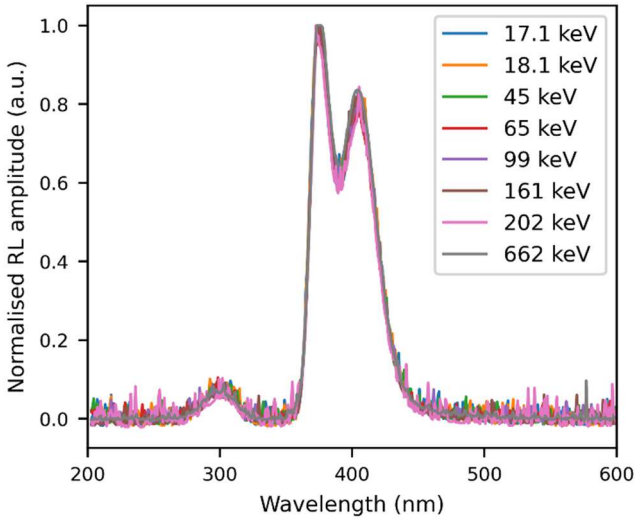


215

216 *Figure 5. Normalized RL emission spectra of CLYC irradiated with X-rays of different energies (mean*
217 *values between 17.1 keV and 202 keV) and with the $^{137}$Cs source (662 keV).*

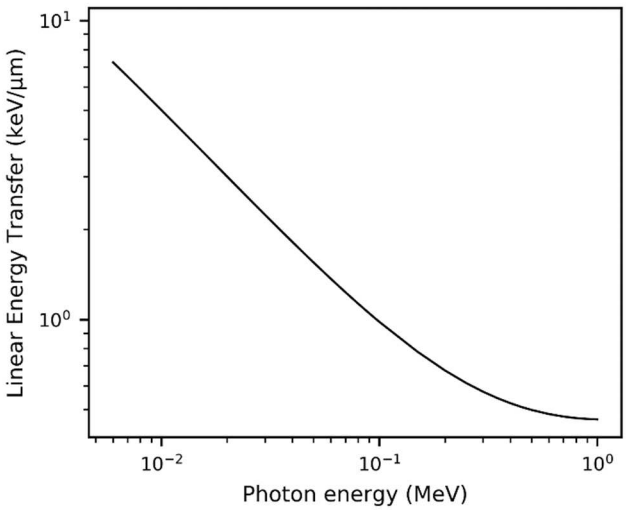


*Figure 6. The LET versus photon energy calculated for the CLYC crystal in the 5 keV – 1 MeV energy region. Data taken from* [29].

RL measurements under neutron irradiation were undertaken using an 888 GBq Am-Be fast neutron source at CERN. The employed readout setup was the same as the one used at the Polytechnic of Milan. A 5 cm thick lead slab was interposed between the neutron source and the crystal to suppress the γ-ray background. In spite of the relatively high activity of the source, the low $^{35}$Cl capture cross section and the low sensitivity of the portable spectrometer prevented the detection of any signal above the instrument noise.

### 3.2 Pulse shape analysis with the ultra-fast H6610 Hamamatsu PMT

The time information was obtained employing the Hamamatsu H6610 PMT. Four experiments were performed: $^{137}$Cs irradiation in bare configuration (*i.e.* CLYC facing the PMT), $^{137}$Cs irradiation in filtered configuration (*i.e.* with the optical filter placed between CLYC and PMT), Am-Be irradiation in bare configuration and Am-Be irradiation in filtered configuration.

In the case of the photon irradiation, all pulses were analyzed by aligning, normalizing and averaging the data under the $^{137}$Cs photopeak at 662 keV, thus obtaining the so-called standard pulse. In the case of Am-Be irradiation, particle discrimination was first performed by PSD using the charge integration method [30]. The collected signals were integrated following the formula:

$$\mathrm{PSD} = \frac{Q_{prompt}}{Q_{prompt}+Q_{tail}} \qquad (1)$$

where $Q_{prompt}$ is the integral charge between the start of integration and 50 ns, and $Q_{tail}$ is the integral charge from 50 ns to 1500 ns. These two values were chosen after the optimization of the PSD Figure Of Merit (FOM = 2.33). The FOM was calculated as following [24]:

$$\mathrm{FOM} = \frac{x_\gamma - x_n}{FWHM_\gamma + FWHM_n} \qquad (2)$$

where $x_\gamma$ and $x_n$ are the mean values of the photon and neutron gaussian distributions of the PSD and $FWHM_\gamma$ and $FWHM_n$ the corresponding full widths at half maximum.

Figure 7 shows the PSD histogram plot, from which the FOM was calculated, and the 2D histogram plot of the PSD versus the total charge in the case of unfiltered Am-Be irradiation. The acquired

signals were then classified in the PSD space, and only those belonging to the neutron region of the PSD space (blue box in the right plot of figure 7) were used for the decay time analysis. The neutron region was defined by the signals with a PSD value within $x_n \pm \sigma_n$, *i.e.* between 0.082 and 0.113, in order to cut the signals in the tails of the Gaussian distribution.
For the sake of completeness, also the signals classified in the PSD space as photons (red box in the right plot of figure 7) were averaged and the corresponding standard pulse was calculated for the decay time analysis.
The uncertainty of the calculated decay time is mainly affected by the number of the averaged signals, the signal alignment and the region selected as neutrons or photons in the 2D PSD histogram plot, whereas the uncertainty on the fitting procedure is negligible.A total uncertainty of 10 % was estimated for the measurements with the PMT.

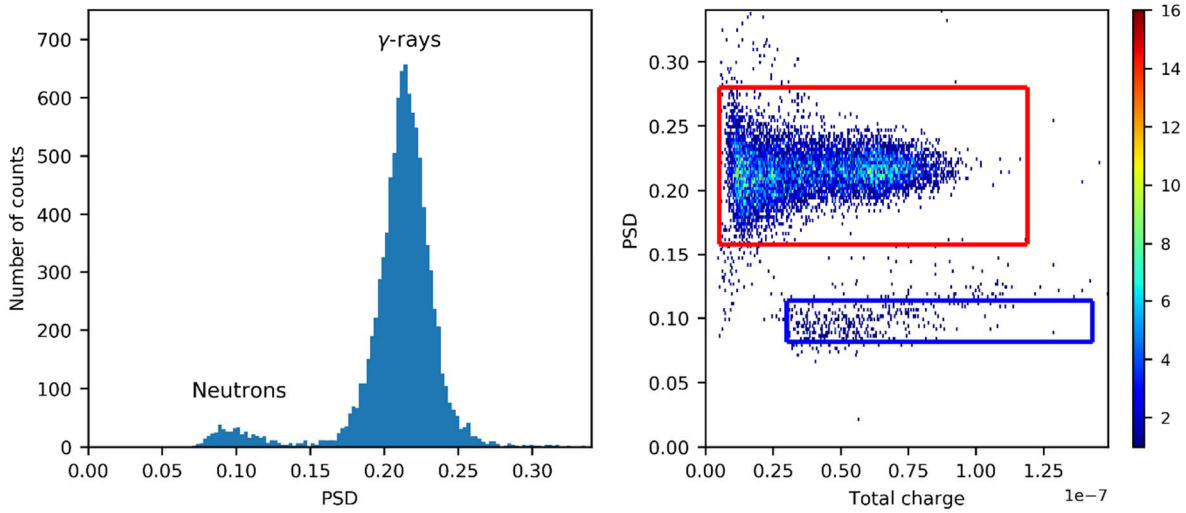


*Figure 7. On the left, the PSD histogram plot calculated for the Am-Be neutron source; on the right, the 2D PSD histogram plot where γ-rays and neutrons are identified by the two regions enclosed in a red and a blue box, respectively.*

As mentioned above, measurements were performed for both the bare and the filtered configuration. However, the filtered results had to be discarded, because the filter did not significantly modify the recorded signals in the case of both γ-ray and neutron irradiations. This result is in contrast with the previous RL measurements, where it was observed that only the emission related to the CVL region was transmitted by the optical filter, and thus an appreciable distortion of the signal was expected. Moreover, the signal amplitude did not vary significantly. Therefore, the filtered results were rejected because of experimental errors (two possible explanations are given in section 4), and hereafter only the unfiltered configuration results are discussed.

The decay curves of the standard pulses were fitted using a sum of four, for γ-rays, and three, for neutrons, exponential decays, according to the following equation:

$$y(t) = \sum_i A_i e^{-t/\tau_i} \qquad (3)$$

where $A_i$ is the amplitude of each exponential and $\tau_i$ the decay time.

Figures 8, 9 and 10 show the standard pulses with the fit and the plot of the residuals calculated as the difference between the experimental and the model predictions. In all cases the fit is satisfactory, with $R^2 \sim 1$; the model does not systematically underestimate/overestimate the

experimental data. The results of the fits are summarized in table 1. The uncertainties reported in table 1 are statistical. For each pulse, the table reports the time constants $\tau_i$ and the relative intensity of the associated scintillation mechanism in relation to the total signal. The relative intensities were calculated as the percent contribution of the single scintillation mechanism to the total signal.

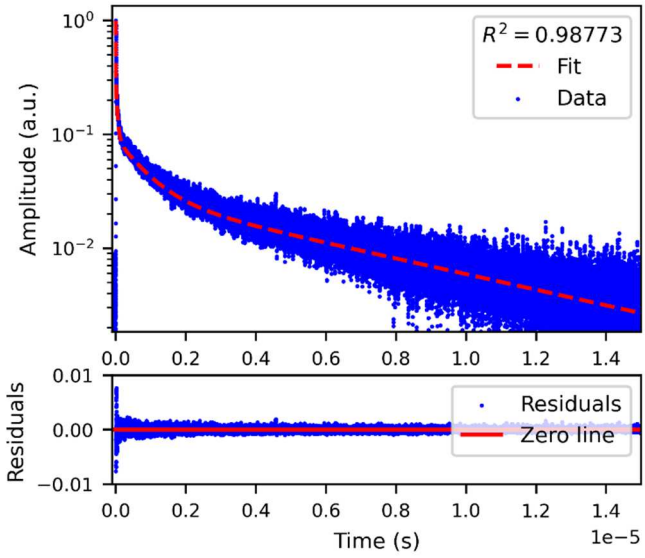


*Figure 8. Top: the standard pulse and the fit of the photon signals for the $^{137}$Cs source irradiation. Bottom: the plot of the residuals.*

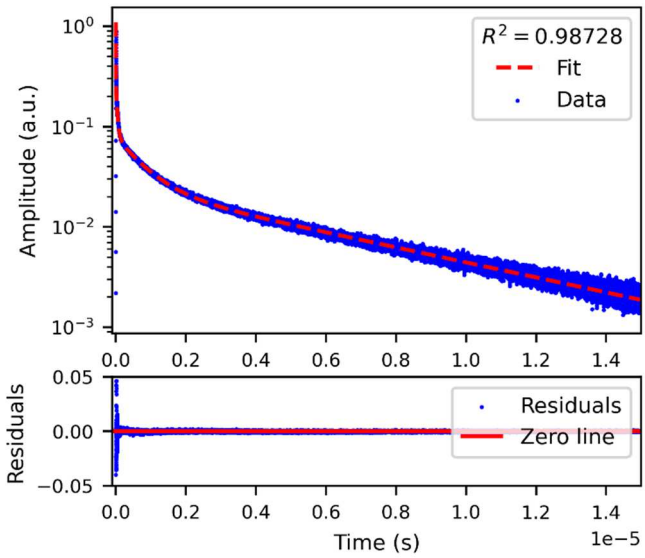


*Figure 9. Top: the standard pulse and the fit of the photon signals for the Am-Be source irradiation. Bottom: the plot of the residuals.*

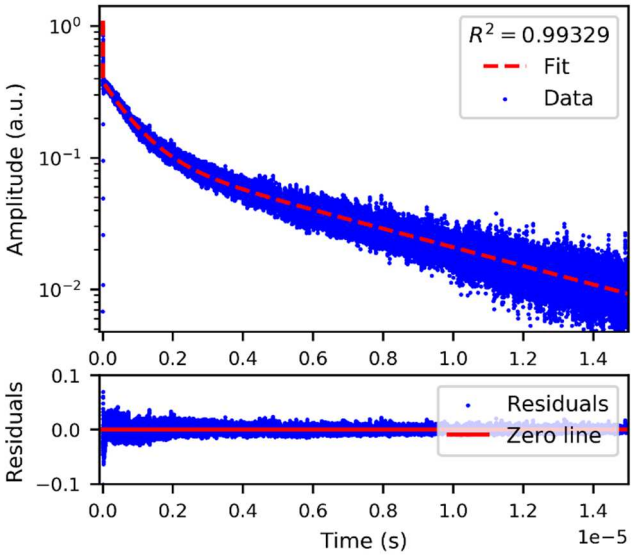


*Figure 10. Top: the standard pulse and the fit of the neutron signals from the Am-Be source irradiation. Bottom: the plot of the residuals.*

*Table 1. The decay times (τ) and the relative intensity (Int) of the CLYC scintillation mechanisms calculated for the standard pulses produced by γ-rays and neutrons. Measurements performed with the Hamamatsu H6610 PMT.*

| Particle (source) | CVL | | Fast $Ce^{3+}$ | | $V_k$ | | STE | | |
|---|---|---|---|---|---|---|---|---|---|
| | $\tau_1$ (ns) | Int (%) | $\tau_2$ (ns) | Int (%) | $\tau_3$ (ns) | Int (%) | $\tau_4$ (ns) | Int (%) | $R^2$ |
| γ-rays ($^{137}$Cs) | $2.7 \pm 0.3$ | 1.10 | $45 \pm 5$ | 3.26 | $781 \pm 78$ | 20.68 | $6325 \pm 633$ | 74.96 | 0.988 |
| γ-rays (Am-Be) | $2.5 \pm 0.2$ | 1.49 | $43 \pm 4$ | 3.70 | $747 \pm 75$ | 21.11 | $5806 \pm 581$ | 73.70 | 0.997 |
| Neutrons (Am-Be) | $1.7 \pm 0.2$ | 0.22 | — | — | $824 \pm 82$ | 25.57 | $6140 \pm 614$ | 74.21 | 0.993 |

As expected, for the γ-ray irradiation four mechanisms were observed, with their estimated coefficients in agreement with the literature, *i.e.* CVL 1-5 ns, direct capture ~ 50 ns, binary recombination mediated by Vk ~ 700 ns and STE ~ 5 µs. In general, literature data agree on the quenching effects of high LET particles on the CVL. The LET of an α particle produced by a neutron reaction from an Am–Be source in CLYC is around 150 keV/µm while it is 15 keV/µm for a proton, *i.e.* 30 and 3 times higher, respectively, than the maximum LET studied in section 3.1. However, the present results show that an ultra-fast scintillation mechanism is also present with neutrons, which was attributed to the CVL. The faster decay time of the CVL with neutrons might be due to the statistical uncertainty of the standard pulse. Nevertheless, a fast decay component is clearly seen from the neutron standard pulse (see figure 10).

According to the present results, the CVL is only partially quenched by neutrons, while the fast decay is completely quenched. In fact, the neutron standard pulse is better fitted by a 3-exponential function rather than a 4-exponential one. The relative importance of the CVL drops from 1.1% with a

4-exponential function in the case of γ-ray irradiation, down to 0.22% with a 3-exponential function in the case of neutron irradiation. This result is not in complete disagreement with literature data. Firstly, the CVL is actually quenched by high LET particles. In addition, the low intensity of the residual CVL might not be observed if the employed setup is not sensitive enough. In the present experiment, the flat spectral response and fast rise time of the Hamamatsu H6610 PMT together with the fast oscilloscope allowed distinguishing between the two contributions (CVL and fast $Ce^{3+}$) even in the case of a strong CVL quenching.

### 3.3 Pulse shape analysis with the Time Correlated Single Photo Counting (TCSPC) setup

Figure 11 shows the results of the TCSPC measurement: the left plot shows the unfiltered configuration, the right plot the filtered one. The points in the histogram are the time measurements with a bin width of 60 ps. The green line is the moving average of the data, the red line is the fit to the data. The plot of the residuals of each pulse is also shown. For a better analysis of the filtered data, figure 12 shows a zoom of the results for the filtered case together with the measured Impulse Response Function (IRF) of the system, *i.e.* the time resolution of the acquisition system. The fitting equation shown in figure 12 was obtained by convolving the IRF with the scintillator response function. The details of the fitting procedure are described in [17]. Figure 12 shows that the contribution of the IRF to the decay component of the measured pulse is negligible. Table 2 reports the decay times $\tau_d$, with their statistical uncertainties and their relative intensity on the total signal. A 0.5 % uncertainty on the calculation of the decay times is due to the TCSPC setup [16], which is negligible with respect to the fitting uncertainty. Thus, the latter is reported in table 2.

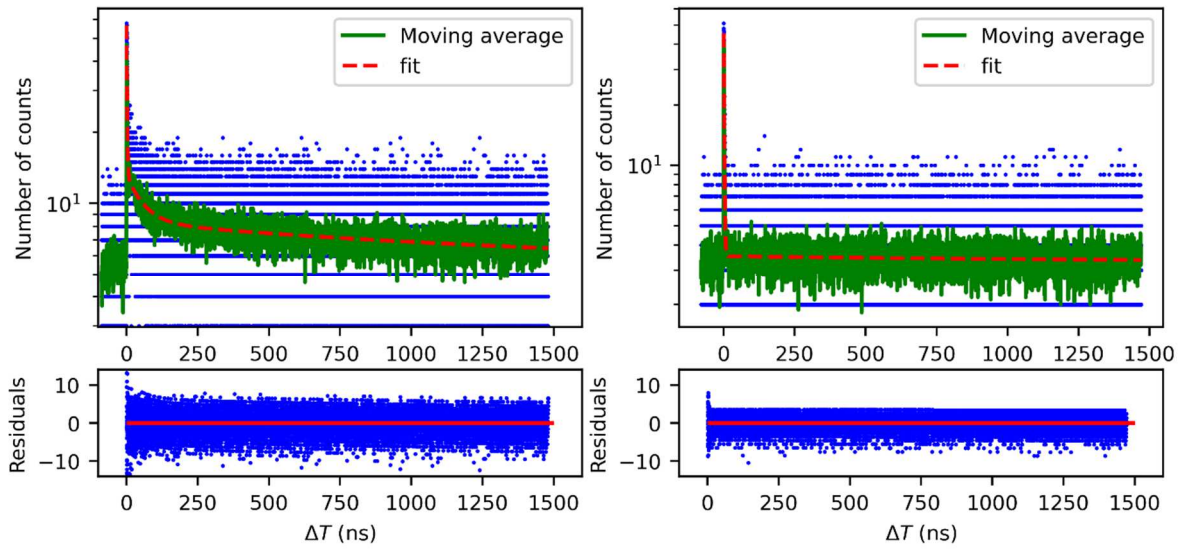


*Figure 11. The result of the TCSPC measurement of the CLYC response without the filter (on the left) and with the filter (on the right). The points are the measured data, the green line is the moving average and the red line is the fit. The bottom plots show the corresponding residuals.*

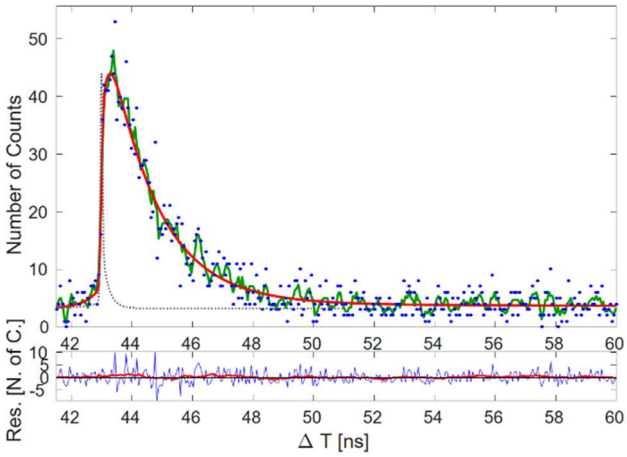


*Figure 12. A zoom of the results of the TCSPC measurement of the CLYC response with the filter. The points are the measured data, the green line is the moving average and the red line is the fit. The dotted black line is the IRF of the system.*

*Table 2. The decay times (τ) and the relative intensity (Int) of the CLYC scintillation mechanisms estimated through the TCSPC technique in both bare and filtered configurations.*

| Setup | CVL | | Fast $Ce^{3+}$ | | $V_k$ + STE | | $\chi^2$ |
|---|---|---|---|---|---|---|---|
| | $\tau_1$ (ns) | Int (%) | $\tau_2$ (ns) | Int (%) | $\tau_3$ (ns) | Int (%) | |
| Unfiltered | $1.90 \pm 0.07$ | 2.06 | $57 \pm 4$ | 6.53 | $1379 \pm 67$ | 91.41 | 1.002 |
| Filtered | $1.67 \pm 0.04$ | 18.58 | — | — | $1639 \pm 482$ | 81.42 | 0.997 |

The decay constants estimated with the TCSPC setup without the filter match reasonably well the decay times measured with the PMT and agree with literature data, taking into account the different recorded length [9,31]. In the filtered configuration the fast emission is dominated by the CVL mechanism, while the $Ce^{3+}$ emission around 50 ns is not detected, so it appears that optical filtration is in line with the RL measurements.

The TCSPC setup is optimized for the estimation of the fastest decay mechanisms of the analyzed scintillator. In particular, its 60 ps discretization and the possibility to introduce the impulse response function of the measurement system in the fit allow precisely estimating extremely fast decay constants [17]. Conversely, the 1500 ns integration window does not permit distinguishing between the two slowest scintillation mechanisms, which are merged in a single $V_k$ + STE component.

### 3.4 Discussion

The different experiments here reported aimed at observing the same scintillation process from different perspectives, *i.e.* in the time and wavelength domains. The RL filtered *vs* unfiltered results can be qualitatively compared to the TCSPC filtered *vs* unfiltered results, respectively. In both cases, the optical filter was placed at a certain distance between the crystal and the sensor without any optical coupling. The RL measurement results showed that no signal was collected at wavelengths longer than the filter cut-off. In the TCSPC experiments, the decay constant of the fast mechanism, which is confined within 350–450 nm wavelength range, completely disappeared.

The merged $V_k$ + STE component becomes appreciably slower with the optical filtration, thus suggesting that also the intermediate component, which is again confined in the $Ce^{3+}$-related region, was blocked by the filter. Literature data and the RL measurement (figure 3) endorse this hypothesis. Thus, the retention of the slower component in the filtered signal can be ascribed to the STE de-excitation since its emission spectrum spans from 240 nm up to 460 nm [11,12,32], even though in large doped crystals the STEs mainly de-excite on $Ce^{3+}$. Therefore, most of the signal belonging to the lower wavelength region appears to be dominated by STE de-excitation instead of CVL (at least > 80% relative importance; the exact value can be obtained with integration windows at least ≥ 15 μs). However, the number of counts of the filtered signal in the tail region is around the background level and its estimation is affected by a major uncertainty. For this reason, the relative intensities of the decay mechanisms in the deep-UV – NUV region cannot be precisely evaluated.

The TCSPC and fast PMT results can be quantitatively compared. The H6610 PMT is particularly fast: its rise and transit times are of the order of tenths of ns. However, considering the 1–5 ns decay constant of the CVL, the PMT response function is expected to perturb the estimation of the decay constant. On the contrary, the 1500 ns integration window allowed distinguishing between the intermediate and the slow components.

Therefore, the two measurements allow estimating different quantities in the bare configuration under γ-ray irradiation, but a correspondence should first be established. To assess the correspondence between the two measurements, one can integrate the fast PMT measurement in the bare configuration under photon irradiation for 1500 ns and compare it to the corresponding TCSPC result. The fit has to be done with the same 3-exponential function of the TCSPC experiment. Table 3 summarizes the obtained fit coefficients with their statistical uncertainty and their relative intensities.

*Table 3: Decay constants (τ) and relative intensities (Int) of the CLYC scintillation mechanisms measured with the TCSPC technique compared to the Hamamatsu H6610 PMT results. In both cases the integration time was 1500 ns.*

| Setup | CVL | | Fast $Ce^{3+}$ | | $V_k$ + STE | |
|---|---|---|---|---|---|---|
| | $\tau_1$ (ns) | Int (%) | $\tau_2$ (ns) | Int (%) | $\tau_3$ (ns) | Int (%) |
| TCSPC | $1.90 \pm 0.07$ | 2.06 | $57 \pm 4$ | 6.53 | $1379 \pm 67$ | 91.41 |
| PMT | $2.8 \pm 0.3$ | 2.04 | $49 \pm 5$ | 6.46 | $1394 \pm 139$ | 91.50 |

The two fits are quantitatively superimposable. The main difference is a 45% discrepancy on the CVL decay constant, which is slower in the case of the fast PMT measurement. The result was expected since the PMT response time is comparable to the CVL decay constant. However, the relative intensity is the same for the PMT and TCSPC measurements. Hence, the four decay coefficients estimated with the fast PMT measurement (see table 2) can be considered sufficiently accurate for estimating the effects of the neutron quenching on the CLYC scintillation mechanisms. Therefore, the conclusions drawn in section 3.2 are further validated, *i.e.* with neutrons the fast mechanism is fully quenched, while the CVL is strongly, but only partially, quenched.

It is worth mentioning that the quenching of the CVL by heavy ions is still under study, especially for relatively new crystals such as CLYC. Most of the authors agree with ascribing this effect to the high excitation density promoted by heavy ions [5,33,34], however its origin is not completely clear. For

example, according to Kirm et al., [33], the quenching of the CVL is due to the higher probability, with increasing LET, of recombination between the electrons of the conduction band with the holes of the core band. This recombination competes with the CVL. Nevertheless, in [34] an ultra-fast scintillation mechanism (< 1 ns), ascribed to the CVL, was actually measured in a $BaF_2$ crystal after heavy ion irradiation.

Finally, the optical filtration operated well in the case of the RL and TCSPC experiments, but no effects were observed during the fast PMT experiments. Two possible explanations are 1) a problem in the measurement setup, *i.e.* inaccurate coupling between crystal and filter, or 2) effects of the optical grease and/or direct coupling between crystal and filter. The second hypothesis is related to the fact that the dichroic filter used is slightly sensitive to both the impinging photon direction and the refractive index of the medium it is in contact with. The filter transmittance was measured in air (figure 3), while during the measurements with the PMT the filter was in between the PMT and CLYC and its surfaces were covered by the optical grease. Further investigations are required, in particular in the light of performing n/γ discrimination using the emission-wavelength information.

## 4. Conclusions

The different experiments performed using the $^{7}$Li enriched crystal and the Asahi optical filter allowed precisely characterizing the material scintillation process. The wavelength-resolved RL results obtained with different photon energies allowed verifying that there is no LET-dependence of the CLYC emission in the range 0.5–5 keV/µm, *i.e.* X-ray and γ-ray stimulations do not significantly distort the CLYC scintillation process.

The fast PMT measurements allowed observing the effects of the neutron quenching in the time domain. Differently from what reported by some authors: 1) a residual CVL signal is observed; 2) the direct electron-hole capture is fully quenched by the neutron capture products. The fast characteristic time and the rather flat quantum efficiency of the PMT allowed distinguishing among the fast and ultra-fast mechanisms also in the presence of a strong CVL quenching.

The TCSPC measurements allowed validating the fast PMT findings. Moreover, the filtered *vs* unfiltered TCSPC experiments suggested that in the 250–330 nm region both the CVL and the host luminescence are present, with a predominant contribution due to the STE de-excitation. However, the relative intensity of these two mechanisms cannot be precisely estimated because of the uncertainty affecting the STE estimation and the short integration window of the TCSPC experiment.

## Acknowledgements

We wish to thank Etiennette Auffray for putting at our disposal the equipment of the Crystal Clear/EP_CMX_DA group for study of the scintillation properties. We also would like to thank the team at FBK for their support and related material used in this study. This project has been partially funded by the CERN Knowledge Transfer fund, through a grant awarded in 2014.

## References

[1] J. Glodo, R. Hawrami, K.S. Shah, Development of Cs2LiYCl6 scintillator, Journal of Crystal Growth. 379 (2013) 73–78. https://doi.org/10.1016/j.jcrysgro.2013.03.023.

[2] J. Glodo, W.M. Higgins, E. V.D. Van Loef, K.S. Shah, Scintillation properties of 1 inch Cs2LiYCl6:Ce crystals, IEEE Transactions on Nuclear Science. 55 (2008) 1206–1209. https://doi.org/10.1109/TNS.2007.913467.

[3] N. Dolympia, P. Chowdhury, E.G. Jackson, C.J. Lister, Fast neutron response of 6Li-depleted

CLYC detectors up to 20 MeV, Nuclear Instruments and Methods in Physics Research, Section A: Accelerators, Spectrometers, Detectors and Associated Equipment. 763 (2014) 433–441. https://doi.org/10.1016/j.nima.2014.06.074.

[4] N. Dinar, D. Celeste, M. Silari, V. Varoli, A. Fazzi, Pulse shape discrimination of CLYC scintillator coupled with a large SiPM array, Nuclear Instruments and Methods in Physics Research, Section A: Accelerators, Spectrometers, Detectors and Associated Equipment. 935 (2019) 35–39. https://doi.org/10.1016/j.nima.2019.04.099.

[5] P.A. Rodnyi, Core-valence luminescence in scintillators, Radiation Measurements. 38 (2004) 343–352. https://doi.org/10.1016/j.radmeas.2003.11.003.

[6] N. D'Olympia, P. Chowdhury, C.J. Lister, J. Glodo, R. Hawrami, K. Shah, U. Shirwadkar, Pulse-shape analysis of CLYC for thermal neutrons, fast neutrons, and gamma-rays, Nuclear Instruments and Methods in Physics Research, Section A: Accelerators, Spectrometers, Detectors and Associated Equipment. 714 (2013) 121–127. https://doi.org/10.1016/j.nima.2013.02.043.

[7] R.H. Pots, E. Auffray, S. Gundacker, Exploiting Cross-Luminescence in BaF2 for Ultrafast Timing Applications Using Deep-Ultraviolet Sensitive HPK Silicon Photomultipliers, Frontiers in Physics. 8 (2020) 482. https://doi.org/10.3389/fphy.2020.592875.

[8] Z.W. Bell, D.E. Hornback, M.Z. Hu, J.S. Neal, Wavelength-based neutron/gamma ray discrimination in CLYC, 2014 IEEE Nuclear Science Symposium and Medical Imaging Conference, NSS/MIC 2014. (2016). https://doi.org/10.1109/NSSMIC.2014.7431197.

[9] B.S. Budden, L.C. Stonehill, J.R. Terry, A. V. Klimenko, J.O. Perry, Characterization and investigation of the thermal dependence of Cs 2LiYCl6: Ce3+ (CLYC) waveforms, IEEE Transactions on Nuclear Science. 60 (2013) 946–951. https://doi.org/10.1109/TNS.2012.2215884.

[10] D. Nesrine, Development of neutron detectors for use in radiation protection, University of Paris-Saclay, 2019.

[11] E. V.D. Van Loef, P. Dorenbos, C.W.E. Van Eijk, K.W. Krämer, H.U. Güdel, Scintillation and spectroscopy of the pure and Ce3+-doped elpasolites: Cs2LiYX6 (X = Cl, Br), Journal of Physics Condensed Matter. 14 (2002) 8481–8496. https://doi.org/10.1088/0953-8984/14/36/307.

[12] P. Dorenbos, Scintillation mechanisms in Ce 3+ doped halide scintillators, Physica Status Solidi (A) Applications and Materials Science. 202 (2005) 195–200. https://doi.org/10.1002/pssa.200460106.

[13] G. Zorloni, F. Cova, M. Caresana, M. Di Benedetto, J. Hostaša, M. Fasoli, I. Villa, I. Veronese, A. Fazzi, A. Vedda, Neutron/γ discrimination by an emission-based phoswich approach, Radiation Measurements. 129 (2019) 106203. https://doi.org/10.1016/j.radmeas.2019.106203.

[14] G. Zorloni, L. Cremonesi, F. Cova, A. Vedda, M. Caresana, Development of a new optical-based quasi-digital particle discrimination technique using inorganic scintillators, Radiation Measurements. 135 (2020) 106370. https://doi.org/10.1016/j.radmeas.2020.106370.

[15] M.N. Ullah, C. Park, E. Pratiwi, C. Kim, H. Choi, J.Y. Yeom, A new positron-gamma discriminating phoswich detector based on wavelength discrimination (WLD), Nuclear Instruments and Methods in Physics Research, Section A: Accelerators, Spectrometers, Detectors and Associated Equipment. 946 (2019) 162631. https://doi.org/10.1016/j.nima.2019.162631.

[16] S. Gundacker, E. Auffray, K. Pauwels, P. Lecoq, Measurement of intrinsic rise times for various L(Y)SO and LuAG scintillators with a general study of prompt photons to achieve 10 ps in TOF-PET, Physics in Medicine and Biology. 61 (2016) 2802–2837. https://doi.org/10.1088/0031-9155/61/7/2802.

[17] S. Gundacker, R.M. Turtos, E. Auffray, P. Lecoq, Precise rise and decay time measurements of inorganic scintillators by means of X-ray and 511 keV excitation, Nuclear Instruments and Methods in Physics Research, Section A: Accelerators, Spectrometers, Detectors and Associated Equipment. 891 (2018) 42–52. https://doi.org/10.1016/j.nima.2018.02.074.

[18] CLYC Gamma-Neutron Scintillator for SPRDs and RIIDs | RMD, Dynasil, (n.d.). https://www.dynasil.com/product-category/scintillators/clyc-gamma-neutron-scintillators/ (accessed May 17, 2021).

[19] Optical Filters and Instruments | Asahi Spectra USA Inc., (n.d.). https://www.asahi-spectra.com/ (accessed May 17, 2021).

[20] Prime™ X, 2011. www.bwtek.com (accessed May 17, 2021).

[21] ISO 4037-1:2019, Radiological protection — X and gamma reference radiation for calibrating dosemeters and doserate meters and for determining their response as a function of photon energy., (n.d.).

[22] HAMAMATSU H6610, (n.d.). https://dtsheet.com/doc/749739/hamamatsu-h6610 (accessed May 17, 2021).

[23] PHOTOMULTIPLIER TUBES AND ASSEMBLIES FOR SCINTILLATION COUNTING & HIGH ENERGY PHYSICS, (n.d.).

[24] F. Anghinolfi, P. Jarron, F. Krummenacher, E. Usenko, M.C.S. Williams, NINO, an ultra-fast, low-power, front-end amplifier discriminator for the Time-Of-Flight detector in ALICE experiment, in: IEEE Nuclear Science Symposium Conference Record, Institute of Electrical and Electronics Engineers Inc., 2003: pp. 375–379. https://doi.org/10.1109/nssmic.2003.1352067.

[25] A. Gola, F. Acerbi, M. Capasso, M. Marcante, A. Mazzi, G. Paternoster, C. Piemonte, V. Regazzoni, N. Zorzi, NUV-sensitive silicon photomultiplier technologies developed at fondazione Bruno Kessler, Sensors (Switzerland). 19 (2019). https://doi.org/10.3390/s19020308.

[26] Introduction to SiPM TECHNICAL NOTE, 2011.

[27] S. Gundacker, R.H. Pots, A. Nepomnyashchikh, E. Radzhabov, R. Shendrik, S. Omelkov, M. Kirm, F. Acerbi, M. Capasso, G. Paternoster, A. Mazzi, A. Gola, J. Chen, E. Auffray, Vacuum ultraviolet silicon photomultipliers applied to BaF 2 cross-luminescence detection for high-rate ultrafast timing applications , Physics in Medicine & Biology. 66 (2021) 114002. https://doi.org/10.1088/1361-6560/abf476.

[28] S. Lam, J. Fiala, M. Hackett, S. Motakef, A High-Performance CLYC(Ce)-PVT Composite for Neutron and Gamma Detection, IEEE Transactions on Nuclear Science. 65 (2018) 609–615. https://doi.org/10.1109/TNS.2017.2779783.

[29] No Title, (n.d.). https://physics.nist.gov/PhysRefData/Star/Text/ESTAR.html (accessed August 18, 2021).

[30] G.F.Knoll, Radiation Detection and Measurements, 4th ed., 2010.

[31] X. Wen, A. Enqvist, Measuring the scintillation decay time for different energy deposited by γ-

rays and neutrons in a Cs2LiYCl6:Ce3+ detector, Nuclear Instruments and Methods in Physics Research, Section A: Accelerators, Spectrometers, Detectors and Associated Equipment. 853 (2017) 9–15. https://doi.org/10.1016/j.nima.2017.02.019.

[32] C.M. Combes, P. Dorenbos, C.W.E. Van Eijk, K.W. Krämer, H.U. Güdel, Optical and scintillation properties of pure and Ce3+-doped Cs2LiYCl6 and Li3YCl6 : Ce3+ crystals, Journal of Luminescence. 82 (1999) 299–305. https://doi.org/10.1016/S0022-2313(99)00047-2.

[33] M. Kirm, A. Lushchik, C. Lushchik, A.I. Nepomnyashikh, F. Savikhin, Dependence of the efficiency of various emissions on excitation density in BaF2 crystals, Radiation Measurements. 33 (2001) 515–519. https://doi.org/10.1016/S1350-4487(01)00044-0.

[34] K. Kimura, LET-, ionic species- and temperature-dependence on Auger-free and self-trapped exciton luminescence of ion-irradiated BaF2 and CsCl single crystals, Nuclear Instruments and Methods in Physics Research Section B: Beam Interactions with Materials and Atoms. 116 (1996) 57–60. https://doi.org/https://doi.org/10.1016/0168-583X(96)00011-0.

# Can the Core-to-Valence Luminescence (CVL) be used to perform n/γ discrimination in a CLYC crystal through optical filtering selection of the scintillation light?

## THE IDEA

### $^{137}$Cs source irradiation

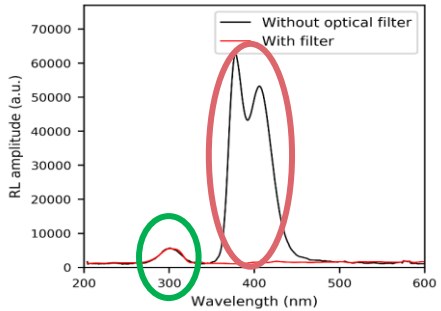


CVL emission — $Ce^{3+}$ emission

- Different wavelength region
- Quenched by high LET particles such as neutron reactions' products.

## IS THE PROPOSED IDEA FEASIBLE?

### Measurements and results

#### X-ray irradiation

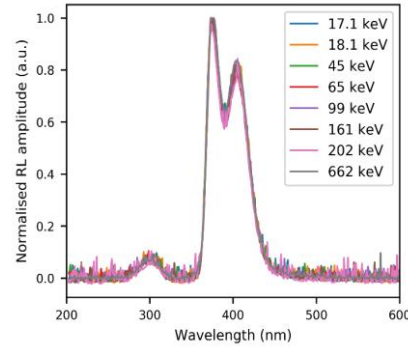


#### Fast Photomultiplier Tube

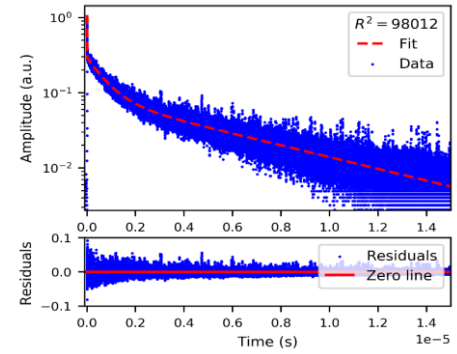


#### Time Correlated Single Photo Counting

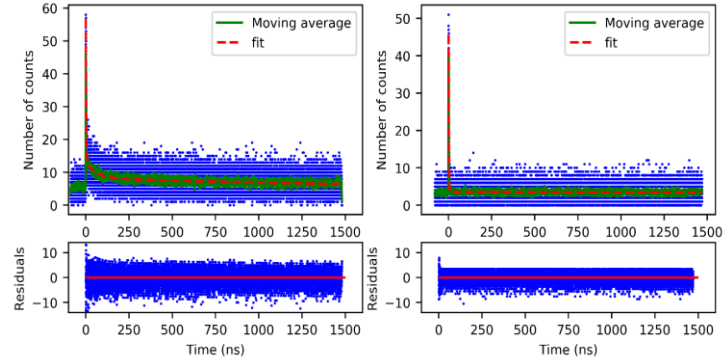


### Conclusions:

- The CVL intensity is constant with photons in the energy range 20-660 keV ✓
- Neutrons partially quench the CVL and completely cut the direct electron-hole capture ✗
- The luminescence in the 250-350 nm wavelength range might be attributed to both the CVL and the host luminescence ✗

F. Ferrulli et al., 2021